Mössbauer and EPR Study of Recombinant Acetyl-CoA Synthase from *Moorella thermoacetica*†

Matthew R. Bramlett,‡,§ Audria Stubna,|| Xiangshi Tan,⊥ Ivan V. Surovtsev,⊥ Eckard Münck,|| and Paul A. Lindahl*,‡,⊥

Department of Biochemistry and Biophysics, Texas A&M University, College Station, Texas 77843, Department of Chemistry, Carnegie Mellon University, Pittsburgh, Pennsylvania 15213, and Department of Chemistry, Texas A&M University, College Station, Texas 77843

Received January 2, 2006; Revised Manuscript Received May 11, 2006

ABSTRACT: Mössbauer and EPR spectroscopies were used to study the electronic structure of the A-cluster from recombinant acetyl-CoA synthase (the α subunit of the $\alpha_2\beta_2$ acetyl-CoA synthase/CO dehydrogenase). Once activated with Ni, these subunits have properties mimicking those associated with the $\alpha_2\beta_2$ tetramer, including structural heterogeneities. The Fe_4S_4 portion of the A-cluster in oxidized, methylated, and acetylated states was in the 2+ core oxidation state. Upon reduction with dithionite or Ti^{3+} citrate, samples of Ni-activated α developed the ability to accept a methyl group. Corresponding Mössbauer spectra exhibited two populations of A-clusters; roughly, 70% contained $[Fe_4S_4]^{1+}$ cubanes, while ∼30% contained $[Fe_4S_4]^{2+}$ cubanes, suggesting an extremely low $[Fe_4S_4]^{1+/2+}$ reduction potential for the 30% portion (perhaps <-800 mV vs NHE). The same population ratio was observed when Ni-free unactivated α was used. The 70% fraction exhibited paramagnetic hyperfine structure in the absence of an applied magnetic field, excluding the possibility that it represents an $[Fe_4S_4]^{1+}$ cluster coupled to a (proximal) Ni_p^{1+}. EPR spectra of dithionite-reduced, Ni-activated α exhibited features at $g = 5.8$ and $g_{ave} \sim 1.93$, consistent with a physical mixture of $\{S = 3/2; S = 1/2\}$ spin-states for A-clusters containing $[Fe_4S_4]^{1+}$ clusters. Incubation of Ni-activated α with dithionite and CO converted 25% of α subunits into the $S = 1/2$ A_{red}-CO state. Previous correlation of this state to functional A-clusters suggests that only the 30% fraction not reduced by dithionite or Ti^{3+} citrate represents functional A-clusters. Comparison of spin states in oxidized and methylated states suggests that two electrons are required for reductive activation, starting from the oxidized state containing Ni_p^{2+}. Refitting published activity-vs-potential data supports an $n = 2$ reductive activation. Enzyme starting in the methylated state exhibited catalytic activity in the absence of an external reductant, suggesting that the two electrons used in reductive activation are retained by the enzyme after each catalytic cycle and that the enzyme does not have to pass through the A_{red}-CO state during catalysis. Taken together, our results suggest that a Ni_p^0 state may form upon reductive activation and reform after each catalytic cycle.

Acetyl-CoA synthases/carbon monoxide dehydrogenases are bifunctional Ni-containing enzymes found in anaerobic archaea and bacteria that grow chemoautotrophically (*1*−*9*).The enzyme from the homoacetogenic bacterium *Moorella thermoacetica* (ACS/CODH[1]) is an $\alpha_2\beta_2$ tetramer that catalyzes reaction 1, the synthesis of acetyl-CoA from CO, coenzyme-A (CoASH), and a methyl group donated from a corrinoid-iron-sulfur protein (CoFeSP). The methyl group originates from methyl-tetrahydrofolate (THF) and is transferred onto CoFeSP according to reaction 2. The methyl group is then transferred as a cation and with inversion to a site on ACS, using an S_N2 type mechanism (*10*, *11*). Apart

$$CH_3Co^{3+}FeSP + CO + CoASH \rightleftarrows CH_3C(O)\text{-}SCoA + Co^{1+}FeSP + H^+ \quad (1)$$

$$Co^{1+}FeSP + CH_3\text{-}THF + H^+ \rightleftarrows THF + CH_3\text{-}Co^{3+}FeSP \quad (2)$$

from generating CO, the β subunit is not involved in the ACS mechanism (*12*). As such, this mechanism and related properties of the A-cluster can be most insightfully studied using the isolated α subunit. Once activated with Ni, recombinant α exhibits methyl group transfer activity and ACS activity (∼10% that of WT ACS/CODH) as long as CO is used as a substrate (*12*, *13*).

† This study was supported by the National Institutes of Health (GM46441 to P.A.L. and EB001475 to E.M.) and the Robert A. Welch Foundation (A1170).

* To whom correspondence should be addressed. Email: Lindahl@mail.chem.tamu.edu; phone, (979) 845-0956; fax, (979) 845-4719.

‡ Department of Biochemistry and Biophysics, Texas A&M University.

§ Present Address: Department of Chemistry, Duke University, P.O. Box 90317, Durham, NC 27708.

|| Carnegie Mellon University.

⊥ Department of Chemistry, Texas A&M University.

[1] Abbreviations: ACS, acetyl-Coenzyme A synthase; CODH, carbon monoxide dehydrogenase; CoASH, coenzyme A, protonated; THF, tetrahydrofolate; EPR, electron paramagnetic resonance; CoFeSP, corrinoid-iron-sulfur protein; WT, wild-type; Ni_p, the proximal Ni of the A-cluster; Ni_d, the distal Ni of the A-cluster; Phen, 1,10-phenanthroline; A-cluster states: A_{ox}, oxidized; A_{red}-CO, reduced and exposed to CO; CH_3-A_{ox}, methylated; $CH_3C(O)$-A_{ox}, acetylated.

10.1021/bi060003+ CCC: $33.50
Published on Web 06/21/2006

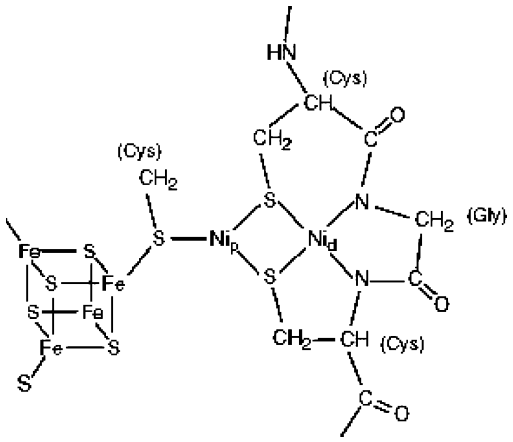

FIGURE 1: Structure of functional A-clusters. See text for details.

The A-cluster is the only metal center in the α subunit and the only redox center evident by X-ray crystallography-(*14*−*16*). Functional A-clusters are composed of an Fe_4S_4 cubane bridged through a cysteinyl sulfur to a Ni ion known as *proximal* Ni_p, which in turn is bridged via two other cysteinyl sulfurs to *distal* Ni_d, a square-planar ion additionally coordinated by two amide nitrogens originating from the protein backbone (Figure 1). Similar N_2S_2 square-planar geometries using carboxamido nitrogen donors stabilize 2+ and 3+ oxidation states of inorganic nickel complexes (*17*−*20*). Since the enzyme operates under anaerobic and reducing conditions, Ni_d is almost certainly in a low-spin 2+ valance in all physiologically relevant states (*2*, *15*), and we shall assume this throughout the paper.

The A-cluster can exist in numerous states. The A_{ox} state is obtained in the absence of reductants and in the presence of chemical oxidants such as thionin (*21*). EPR and Mössbauer spectroscopy reveal that the $[Fe_4S_4]$ cluster in this state is diamagnetic and has a 2+ core valence. The absence of an EPR signal associated with A_{ox} suggests that Ni_p in this state is also in the 2+ valence; thus, the electronic distribution of A_{ox} appears to be $\{[Fe_4S_4]^{2+}\ Ni_p^{2+}\}$. Using K- and L-edge X-ray absorption spectroscopy as well as MCD spectroscopy, Cramer, Grahame, and co-workers have examined the A-cluster-containing subunit in the ACS-related enzyme from *M. thermophila* (*22*, *23*). The two Ni ions of this as-isolated subunit were assigned as Ni^{2+} (50% low-spin $S = 0$ and 50% high-spin $S = 1$), with Ni_p in the high-spin configuration and Ni_d in the low-spin configuration.

The A_{red}-CO state in the α subunit is obtained upon exposure to CO and a low-potential reductant such as dithionite or Ti^{3+}citrate (*21*, *24*, *25*). This $S = 1/2$ state exhibits the *NiFeC* EPR signal, so named because it broadens by magnetic hyperfine interactions when cells are grown on ^{61}Ni or ^{57}Fe, or when the enzyme is exposed to ^{13}CO (*26*−*28*). The A_{red}-CO state of the A-cluster is the only state of the A-cluster for which exchange-coupling between the $[Fe_4S_4]$ cluster and Ni_p^{1+} has been established (*21*). This state has been assigned as $\{[Fe_4S_4]^{2+}\ Ni_p^{1+}\text{-CO}\}$, suggesting that it is obtained when A_{ox} is reduced by 1 electron and bound with CO, as shown in reaction 3.

$$\{[Fe_4S_4]^{2+}\ Ni_p^{2+}\} + 1e^- + CO \rightleftarrows \{[Fe_4S_4]^{2+}\ Ni_p^{1+}\text{-CO}\} \quad (3)$$

One puzzling feature of this enzyme is its heterogeneous nature, initially indicated by the low-spin concentration of the NiFeC signal, which typically quantifies to only ca. 0.1−0.3 spin/α (*29*−*34*). The ability to remove 0.2−0.3 Ni/αβ using 1,10-phenanthroline and to reinsert this fraction upon addition of $NiCl_2$ to phen-treated ACS/CODH demonstrates a connection between Ni lability and low-spin concentration. Most importantly, the inactivity of the phen-treated enzyme and the activity of the Ni-reconstituted enzyme suggest the occurrence of two types of A-clusters called *functional* and *nonfunctional*, where only the functional portion contains labile Ni and can attain the A_{red}-CO state. Further evidence for heterogeneity came from Mössbauer spectra of α subunits in the A_{red}-CO state, which consisted of a paramagnetic component representing 30%−40% of the Fe_4S_4 clusters as well as a diamagnetic component representing 60%−70% of the Fe_4S_4 (*21*). The paramagnetic component originates from the portion of the A-clusters that is functional and exhibits the NiFeC signal, while the diamagnetic component arises from nonfunctional A-clusters. Confirmatory evidence for heterogeneity of the A-cluster was subsequently revealed by one of the X-ray crystal structures of the enzyme, in which only one α subunit per $\alpha_2\beta_2$ tetramer contained Ni_p; the other subunit contained Zn in that site (*15*). Another structure of the enzyme showed Cu ions in both proximal sites (*14*), while a monomeric form showed Ni in the proximal site (*16*). Whether this tendency to replace Ni with Cu or Zn is fundamentally or solely responsible for the heterogeneity remains uncertain, but there can be no doubt that A-cluster populations *are* heterogeneous, with ∼ 30% functional and ∼70% nonfunctional forms. This heterogeneity exists not only for ACS/CODH expressed in its natural host (*M. thermoacetica*) but also in the recombinant enzyme as expressed in *Escherichia coli* (*12*).

Another characterized state of the A-cluster has a methyl group bound and will be called CH_3-A_{ox}. It is not associated with an EPR signal, suggesting a state that has either integer spin or is diamagnetic (*35*, *36*). This state has not been studied by Mössbauer spectroscopy. The CH_3-A_{ox} state appears to be a catalytic intermediate, as subsequent addition of CO and CoASH leads to formation of acetyl-CoA (*36*, *37*). Addition of CO to enzyme in this state is thought to afford the acetylated intermediate (*35*−*38*), to be called CH_3-C(O)-A_{ox}. This state also appears to be EPR silent (*35*−*37*).

The existence of a reductively activated state is implied (but not proven) by the inability of A_{ox} to accept a methyl cation from CH_3-Co^{3+}FeSP *and* by the ability of the A-cluster to accept this group in the presence of a low-potential reductant such as dithionite or Ti^{3+}citrate (*36*, *39*, *40*). This state has not been well-characterized spectroscopically but appears critical for understanding the ACS catalytic mechanism. A major issue in understanding this mechanism is whether this state is 1 or 2 electrons more reduced than A_{ox}. A dithionite-reduced catalytically inactive sample of α was examined previously by Mössbauer spectroscopy and was found to contain all Fe_4S_4 clusters in the 1+ state, apparently all in an $S = 3/2$ form (*21*). Although this sample exhibited no catalytic activity itself, this result nevertheless suggests that reductively activated enzyme is 1-electron more reduced than A_{ox}, with the additional electron localized on the cubane. ACS/CODH must also be reductively activated, and plots of catalytic rates versus solution potential reportedly

fit to the Nernst equation assuming $n = 1$ (*38*, *41*). To the contrary, the EPR-silence of the oxidized and methylated states argues for a 2-electron reductive activation (*36*).

Another unresolved issue is *where* on the A-cluster the electrons or electron localize(s) (*6*). One-electron reduction of Ni_p^{2+} to the 1+ state (in the absence of CO) has been proposed (*23*, *42*), but no EPR signal appropriate for a d^9 $S = 1/2$ ion has been reported for samples reduced with dithionite or Ti^{3+}citrate. Two-electron reduction of Ni_p^{2+}, generating an unprecedented Ni_p^0 state, has also been proposed (*2*, *15*). Brunold has suggested that one electron localizes on the $[Fe_4S_4]$ cluster and one on Ni_p forming a $\{[Fe_4S_4]^{1+}\ Ni_p^{1+}\}$ state (*43*). Ragsdale has proposed that an $n = 1$ redox mediator donates an electron to the A-cluster at one step of catalysis and accepts an electron at another. This redox shuttle was initially thought to be located in the β subunit and to correspond to the C-cluster (*37*), but the catalytic activity of isolated α subunits and the absence of redox centers in the α subunit other than the A-cluster imply that this shuttle, if it indeed exists, should be *external* to the enzyme. This latter possibility is supported by the fact that all enzyme assays reported to date have been carried out in the presence of low-potential reductants (Ti^{3+}citrate or reduced methyl viologen). Ragsdale has recently suggested that a ferredoxin serves this role *in vivo* and has identified a possible docking site on ACS (*6*).

In this paper, we have reexamined various A-cluster states using Mössbauer and EPR spectroscopy with the aim of obtaining additional insight into these unresolved issues. In the previously published Mössbauer study of the α subunit (*21*), this subunit was generated by subjecting native $\alpha_2\beta_2$ ACS/CODH to the detergent SDS, followed by polyacylamide gel electrophoresis and electroelution. This was a rather harsh and difficult procedure such that resulting α subunit preparations were catalytically inactive and could not be methylated. In the current study, the α subunit is obtained by recombinant methods. When prepared in this manner, the α subunit exhibits some catalytic activity (ca. 10% of WT enzyme) and methyl group transfer activity (*12*, *13*). Thus, the results obtained here should be more mechanistically relevant than those obtained previously. Our results clarify the electronic and magnetic properties of the oxidized, methylated, and acetylated states, and they shed new light on the properties of the reductively activated state. Overall, they favor a 2-electron activation of the oxidized A_{ox} state in which both electrons localize on noncubane portions of the A-cluster. Given that Ni_d^{2+} is probably unable to accept one or both of those electrons, our results offer support for the hypothesis that Ni_p^{2+} is reductively activated to a zero-valent state. Another experiment presented suggests that an external reductant is not required for catalytic activity (though it certainly is required for activation). Our results also show that the A_{red}-CO state is not a required catalytic intermediate.

EXPERIMENTAL PROCEDURES

Preparation of Recombinant α Subunit. Plasmid pLHK04, containing the gene *acsB* (similar to pLHK05 (*12*) but lacking the His-tag), was transformed into *E. coli* strain JM109 cells (Stratagene). Cells were grown and expressed as described (*12*) and were harvested in a continuous-flow centrifuge (Heraeus, Contifuge 17RS) inside of an anaerobic glovebag (Coy Laboratories). All subsequent manipulations were carried out in gloveboxes (either Braun Labmaster 130s or Vacuum Atmospheres HE-453-2s) maintained at ≤1 ppm O_2 as continuously monitored (Teledyne model 310). Cells were thawed, resuspended, and stirred in Buffer A (50 mM Tris, pH 8, 10 mM DTT, and 2 mM dithionite) containing 100 mg of lysozyme and a small amount of DNase I (Sigma) for 1.5 h. The cell suspension was poured into liquid-N_2-chilled aluminum cups and sonicated (Branson sonifiers, 60% duty cycle, output 7, 6−7 min per cup) inside of a refrigerated anaerobic glovebox (MBraun). Lysed cells were centrifuged (Sorvall RC-5 plus, GSA rotor, 12 500 rpm, 5 °C, 1.5 h), and the supernatant was loaded onto a 100 mL column of DEAE-Sepharose Fast Flow (Amersham Biosciences) equilibrated in Buffer A, and then washed with 300 mL of Buffer A containing 0.15 M NaCl. Protein was eluted by a gradient of 0.15−0.4 M NaCl in Buffer A. Fractions containing α were identified by SDS−PAGE (Bio-Rad Ready Gels), pooled, and made 0.3 M in ammonium sulfate. This solution was loaded onto 100 mL of Phenyl-Sepharose 6 Fast Flow (low sub, Amersham Biosciences) equilibrated with Buffer A plus 0.3 M ammonium sulfate. After washing with 300 mL of the same buffer, the protein was eluted with a gradient of Buffer A plus 0.3 M ammonium sulfate to Buffer A. Fractions containing α were identified by SDS−PAGE, pooled, and concentrated in stirred cell (Amicon) using a 30 kDa membrane. Final purity (85%) was determined by SDS−PAGE densitometry (Alpha Imager). Acetyl-CoA synthase activity (4 min^{-1}) was determined as described (*12*, *13*).

Preparation of Other Substrates and Redox Mediators. Co^{1+}FeSP, CH_3-Co^{3+}FeSP, and the methyltransferase (MeTr) were purified or prepared as described (*36*). Ti^{3+}citrate was prepared as described (*44*). Sodium dithionite (Sigma) was dissolved in 0.2 M NaOH inside a glovebox and diluted with 50 mM Tris, pH 8, before use. Reductant normalities were standardized against a solution of 50 mM $K_3Fe(CN)_6$. Protein concentrations were determined by the Biuret method (*45*).

Preparation and Characterization of ^{57}Fe-Enriched Recombinant α Subunit. Recombinant α subunit was prepared as described above except that the yeast extract and tryptone used in the growth media were suspended in 2 L of distilled deionized water, autoclaved, and then passed through Chelex-10 resin (Bio-Rad). The solution was combined with other media ingredients, excluding natural-abundance Fe but including 20 μM ^{57}Fe, and then re-autoclaved. After harvesting, cells were resuspended twice with 500 mL of 50 mM Tris, pH 8.0, and then spun down to remove excess ^{57}Fe. The protein was purified and activated as above. Purity was 70%. A portion of the recombinant α was used without Ni-activation. Samples were treated as described in the text and frozen inside of the glovebox by placement on a liquid-nitrogen-cooled Al surface. Samples were digested in 1 M HNO_3 (Fisher, Trace Metal Grade) and then analyzed on a Perkin-Elmer Graphite Furnace AAnalyst 700 Spectrometer. The sample contained 4.7 Fe/α, assuming that none of the contaminating proteins contained Fe. Samples were analyzed by X-band EPR on a Bruker EMX spectrometer using a Hewlett-Packard 5352B microwave frequency counter, the ER4102ST cavity, and the Oxford Instruments ESR900 cryostat. Parameters were as follows: power, 80, 20, or 0.05 mW; modulation amplitude, 12 G; frequency, 9.44 GHz;

conversion time, 163 ms; temperature, 10, or 130 K. Mössbauer spectra were collected on a constant acceleration spectrometer, using two cryostats that allowed studies at 4.2 K in applied fields up to 8.0 T. Isomer shifts are quoted relative to Fe metal at 298 K. Spectra were analyzed with the WMOSS software package (WEB Research Co., Edina, MN).

Ni Activation, Reduction, and Methylation of the α *Subunit*. As-isolated recombinant α was freed of dithionite by passage over a Sephadex G-25 column equilibrated in 50 mM Tris, pH 8. Three to four equivalents of $NiCl_2$ were incubated with reductant-free α for 2−3 h. Activated α was concentrated and passed through a G-25 column to remove excess $NiCl_2$. For reduction by Ti^{3+} citrate, methyl transfer ability was assessed by stopped-flow. One syringe contained 10 μM α and 5 or 40 μM Ti^{3+} citrate; the other syringe contained 5 μM CH_3-Co^{3+}FeSP and the same concentration of Ti^{3+} citrate as in the other syringe; thus, resulting solutions after mixing contained 1 and 8 equiv per α of Ti^{3+} citrate. On the basis of the results obtained, 0.5 and 1.0 equiv/α of Ti^{3+} citrate were added to ^{57}Fe-enriched α. Samples were frozen within ca. 5 min, which is sufficiently long for full reduction (*13*).

Experiment of Figure 3. Activated recombinant α was reduced using a double-septa-sealed quartz cuvette. While in the glovebox, both septa were pierced with the needle of a syringe containing a standardized 11.9 mM dithionite solution. The apparatus was removed from the box and inserted into a UV−visible spectrometer (Beckman DU 640B). Dithionite was injected and rapidly mixed immediately prior to acquiring kinetic traces. The extinction coefficient of dithionite was measured at 316 nm to be 6.35 mM^{-1} cm^{-1}. Methyl-transfer activity of the α subunit was measured as described (*46*), except that dithionite was the reductant and CH_3-Co^{3+}FeSP was reductant-free. Final concentrations of α and CH_3-Co^{3+}FeSP after mixing were 30 and 15 μM, respectively.

Acetyl-CoA Synthesis in the Absence of a Reductant. A stock solution of α was reduced by 2 equiv/α of dithionite and then split into two aliquots. One aliquot was immediately mixed with CH_3-Co^{3+}FeSP, and the solution was incubated at room temperature in the dark. Immediately after mixing, the concentrations of α and CH_3-Co^{3+}FeSP were 60 and 140 μM, respectively. The second aliquot of α was diluted to 60 μM and then mixed at various times with CH_3-Co^{3+}FeSP by the stopped-flow method outlined above. Once methyl-transfer activity ceased, the first aliquot was made 350 μM in CoA and flushed with 1 atm CO. After 45 min incubation in the dark, the sample was removed from the glovebox and concentrated using a 30 kDa microcon (Amicon). The protein-free filtrate was mixed with an equal volume of 1 M citrate, pH 4.8, diluting protein concentrations in half. Fifty microliters of the resulting solution was analyzed by reversed-phase HPLC on a C_{18} column (Varian Chromsep SS 250 mm × 4.6 mm).

Preparation of ^{57}Fe-Enriched Samples. Fourteen samples of ^{57}Fe-enriched α subunit were prepared for this study. Each is designated by *S*, followed by a counter number (01−14). Following this, in parentheses, is the activation (activated or unactivated), redox (thionin-oxidized, dithionite-reduced, Ti^{3+}citrate-reduced, or no redox agents), and substrate (methylated, carbonylated, acetylated, or no substrates) status of the sample.

S01 (Unactivated, No Redox Agents, No Substrates). Recombinant α as purified initially.

S02 (Activated, No Redox Agents, No Substrates). This sample was equivalent to S01, but activated as described above.

S03 (Activated, Dithionite-Reduced, Methylated). An activated sample methylated by adding 20 equiv/α of dithionite followed immediately (within 4 min) by 0.5 equiv/mol of CH_3-Co^{3+}FeSP. Half of this sample was frozen within 20 min; this portion is called *S03*.

S04 (Activated, No Redox Agents, Methylated). This is the other half of the sample just described, frozen after a 20 h incubation which should have been sufficient for the dithionite to have been exhausted (we show below that dithionite is spontaneously consumed by the α subunit after such a lengthy incubation).

S05 (Activated, Thionin-Oxidized, No Substrates). Ni-activated α treated for 1 h with 10 equiv/α of the oxidant thionin. A small portion was diluted 10 times in oxidant-free buffer and examined by optical spectroscopy. It exhibited a spectral feature near 600 nm due to excess thionin, confirming that the sample was fully oxidized when frozen.

S06 (Activated, Dithionite-Reduced, Acetylated). S03 was thawed, immediately exposed to 1 atm CO, and refrozen immediately. This treatment should have resulted in the acetyl-bound state under reducing conditions.

S07 (Activated, No Redox Agents, Acetylated). S04 was thawed, immediately exposed to 1 atm CO, and refrozen immediately. This treatment should have resulted in the acetyl-bound state under nonreducing conditions.

S08 (Unactivated, Dithionite-Reduced, No Substrates). Unactivated α reduced with 20 equiv/α of dithionite and frozen ∼2 min after mixing.

S09 (Activated, Dithionite-Reduced, No Substrates). Activated α subunits reduced with 20 equiv/α of dithionite and frozen ∼2 min after mixing.

S10 (Activated, Dithionite-Reduced, No Substrates). A sample of activated α was transferred to a UV−vis cuvette, reduced with 20 equiv/α of dithionite, and monitored at 316 nm. Slightly less than half of the sample was immediately transferred to a Mössbauer cuvette and frozen immediately to generate *S10*. Subsequent analysis of the remaining solution confirmed that *S10* was methylatable at the time of freezing.

S11 (Activated, No Redox Agents, No Substrates). Five hundred minutes after adding the dithionite, and after it was verified the remainder of the sample just described was unable to accept a methyl group, the bulk of this sample was frozen, generating *S11*. Thus, *S11* should be oxidized.

S12 (Activated, Ti^{3+}Citrate-Reduced, No Substrates). Activated α reduced with 1.0 molar equivalents of Ti^{3+}citrate per α.

S13 (Activated, Ti^{3+}Citrate-Reduced, No Substrates). Activated α reduced with 0.5 molar equivalents of Ti^{3+}citrate per α.

S14 (Activated, Dithionite-Reduced, Carbonylated). Ni-activated α reduced with 20 equiv/α of dithionite and exposed to 1 atm CO.

Fitting Activity versus Potential Data. Data on the redox-dependent enzyme activity from Bhaskar et al. (*38*) were

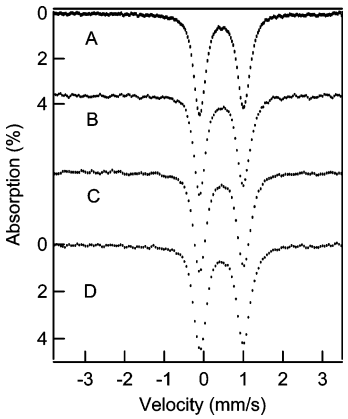

FIGURE 2: The 4.2 K Mössbauer spectra recorded in 50 mT applied fields. (A) *S01* (unactivated, no redox agents, no substrate); (B) *S02* (activated, no redox agents, no substrate); (C) *S03* (activated, dithionite-reduced, methylated); (D) *S04* (activated, no redox agents, methylated).

fitted to determine the number of electrons involved in reduction process. The Nernst equation in the form

$$\frac{E_{act}}{E_{tot}} = \frac{C}{1 + e^{(\Delta E - E_0)(nF/RT)}}$$

was used for fitting simultaneously to three experimental datasets for different pH with number of electrons n as a shared parameter (the same for all theoretical curves). E_0 and proportionality coefficient C were the other parameters varied during fitting procedure (values not shared for different pH). Fitting was performed using Origin 7.5 software (Origin Lab Co; http://www.originlab.com).

RESULTS

Mössbauer Spectra of Oxidized and Methylated α *Subunit.* We prepared seven samples of the α subunit in which the cubane of the A-cluster was present in the 2+ core oxidation state; characteristic spectra are presented in Figure 2. They are indistinguishable from those reported for the oxidized α subunit by Xia et al. (*21*); both sets of spectra display a quadrupole doublet characteristic of $[Fe_4S_4]^{2+}$ clusters, with $\Delta E_Q \approx 1.08$ mm/s and $\delta \approx 0.45$ mm/s. Thus, spectra of *S05* (activated, thionin-oxidized, no substrates) are not shown. Comparison of spectrum 2A from *S01* (unactivated, no redox agents, no substrate) to spectrum 2B from *S02* (activated, no redox agents, no substrate) indicates that the cubane of the A-cluster is not sensitive to the occupancy of the proximal and distal metal binding sites in these oxidized redox states. Similarly, comparison of spectrum 2C from *S03* (activated, dithionite-reduced, methylated) to spectrum 2D from *S04* (activated, no redox agents, methylated) reveals that the cubane is not sensitive to the methylation status of the A-cluster. Comparable spectra from *S06* (activated, dithionite-reduced, acetylated) and *S07* (activated, no redox agents, acetylated) were indistinguishable from those of Figure 2, again indicating that the cubane is not sensitive to the acetylation status of the A-cluster. Most importantly, spectra C and D (and analogous spectra from *S06* and *S07*) exhibited no magnetic hyperfine interactions, a result which has implications for the electronic configuration of the methylated and acetylated forms of the enzyme. Perhaps the most unexpected result of this group of experiments is the presence of an $[Fe_4S_4]^{2+}$ cubane in dithionite-reduced samples (as shown below, reduction by dithionite in the absence of CH_3-Co^{3+}FeSP results in a substantial proportion of reduced $[Fe_4S_4]^{1+}$ cubanes).

Dithionite Consumption by the α *Subunit and Correlation of Reductant Status with Methylation Ability.* In the course of the present study, we discovered that dithionite is consumed catalytically in solutions of α.[2] Consumption was monitored at 316 nm where dithionite absorbs. In a typical experiment, the intensity of this feature began to decline immediately after dithionite and α were mixed, and then it stabilized after ~1 h. Consumption appears catalytic, as repeated additions of dithionite to the same solution of α caused repetition of the same behavior. Similar behavior was observed using recombinant α that had not been activated with Ni and with recombinant Ni-activated α that had been methylated. Thus, Ni_p does not appear to be required for this α-dependent catalytic consumption of dithionite. Control experiments with an equivalent amount of dithionite added to buffer alone showed a slow and monotonic decline at 316 nm, indicating that the rapid and nonlinear consumption of dithionite seen when α was present reflects an α-dependent process.

This consumption of dithionite prompted us to correlate the reductant status of α-containing solutions to the methylation ability of α. We treated a sample of α with 2 equiv/α of dithionite; half was monitored as above for the consumption of dithionite (Figure 3, top panel), while the other was transferred into a stopped-flow syringe and reacted with CH_3-Co^{3+}FeSP at different times. Stopped-flow reactions were monitored at 390 nm which reflects the Co^{1+}FeSP product. Arrows above the 316 nm kinetic trace in the top panel of Figure 3 indicate the times at which the methyl group transfer reaction was initiated. The trace shows an initial sharp decline in absorbance followed by a slight recovery and a plateauing effect. The slight recovery of absorbance probably reflects the oxidation of another chromophore (probably $[Fe_4S_4]^{1+}$ clusters) as dithionite is consumed. Stopped-flow traces revealed that α subunits in solutions containing excess dithionite could accept a methyl group (Figure 3, bottom panel, traces A and B) and that solutions devoid of dithionite and incubated for a long period (Figure 3, bottom panel, trace E and to some extent trace D) could not. The quantified amount of methyl group transferred in this experiment is somewhat low (only ca. 0.1 methyl groups transferred per α), but we use these traces only to assess how the reductant status of the solution correlates with methylation ability. Adding more dithionite to this sample reestablished methylation ability (Figure 3, trace F), confirming that the functional α subunits in trace E were *fundamentally* capable of accepting a methyl group but were not reductively activated in trace E.

Using this approach, we prepared an ^{57}Fe-enriched, Ni-activated sample of the α subunit that was verified to be in

[2] We suspect that the α subunit catalyzes the consumption of dithionite similar to the manner in which the Fe_4S_4-containing Fe protein of nitrogenase does so. In the latter case, dithionite is thought to disproportionate catalytically into SO_3^{2-} and $S_2O_3^{2-}$ without generating H_2 (*63*, *64*). The Fe protein self-oxidizes from the $[Fe_4S_4]^{1+}$ to the $[Fe_4S_4]^{2+}$ state after dithionite is exhausted. Since the α subunit also contains an Fe_4S_4 cluster, it is reasonable to suspect that a similar process is occurring with this protein.

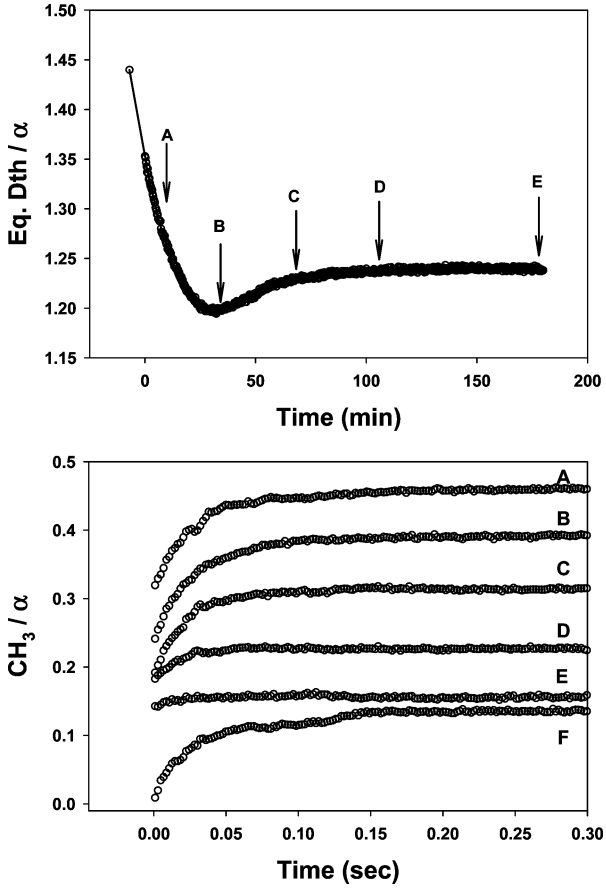

FIGURE 3: Reductant status in α solutions correlated with methylation ability. Top panel, plot of absorbance (316 nm) of reductant-free α subunit (60 μM) vs time after adding 2 equiv/α of dithionite. Bottom panel, stopped-flow traces of the same α subunit solution after reacting with 30 μM CH_3-Co^{3+}FeSP. Arrows indicate times at which stopped-flow traces were obtained, including A, 10; B, 37; C, 70; D, 113; and E, 185 min. After trace E was obtained, an additional 2 equiv/α of dithionite was added to the α solution in the stopped-flow syringe and another trace (F) was then obtained.

a methylatable state (*S10*) and a matched sample (where the dithionite had been exhausted) verified to be in a non-methylatable state (*S11*). A sample of dithionite-reduced, ^{57}Fe-enriched, *unactivated* α (*S08*) and the same material after Ni-activation (*S09*) were also prepared.

After performing the previous dithionite-based experiments, we discovered that Ti^{3+}citrate can also be used for reductive activation and that this reductant is not consumed catalytically like dithionite. This allowed stopped-flow experiments in which reductant-free α subunit was incubated in a buffered solution that contained small molar amounts of freshly prepared and standardized Ti^{3+} citrate and reacted against a solution of CH_3-Co^{3+}FeSP that had also been incubated in the same Ti^{3+} citrate and at that same concentration. When 1 and 8 equiv/α of Ti^{3+} citrate were used for the reduction, 0.35 and 0.40 methyl groups/α transferred from CH_3-Co^{3+}FeSP to α, respectively. Taking into account the heterogeneity, the quantity of methyl groups transferred is as expected for full methyl group transfer to functional A-clusters (*13*, *36*, *46*). The nearly equivalent number of methyl groups transferred in the former case indicates that 1 equiv/α of Ti^{3+} citrate is nearly sufficient for reducing a population of α subunits for full methylation. Analogous ^{57}Fe-enriched α samples were prepared using 0.5

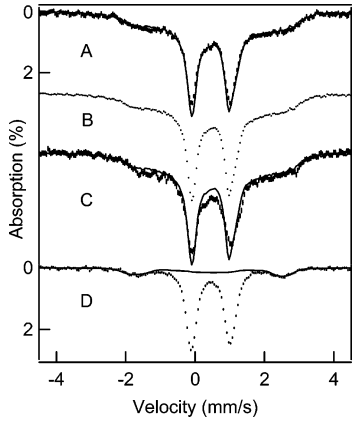

FIGURE 4: Mössbauer Spectra of Reduced α Subunits Recorded at 4.2 K in Applied Fields of 50 mT. (A) *S08* (unactivated, dithionite, no substrates); (B) *S10* (activated, dithionite, no substrates); (C) *S12* (activated, Ti(III)citrate, no substrates); (D) *S14* (activated, dithionite-reduced, CO). For spectral comparison, we have drawn (solid line) through the data (hash marks) of spectra A and C the spectrum of B. The solid line in spectrum D is a spectral simulation of the NiFeC species (25% of total Fe) generated with the spin Hamiltonian parameters of Xia et al. (*21*).

and 1.0 molar equivalents of Ti^{3+} citrate per α, generating samples *S13* and *S12*.

Mössbauer and EPR Spectra of Reduced α Subunit. All of the five reduced samples described above, including *S08*, *S09*, *S10*, *S12*, and *S13* were examined by Mössbauer spectroscopy, and characteristic spectra, recorded at 4.2 K in 50 mT applied fields, are shown in Figure 4, spectra A−C. The previously studied state A_{red}-CO was also prepared using the same preparation of enzyme (*S14*) and examined by Mössbauer spectroscopy (Figure 4D). Spectra A−C, from *S08* (unactivated, dithionite, no substrates), *S10* (activated, dithionite, no substrates), and *S12* (activated, Ti(III)citrate-reduced, no substrates), are very similar; all consist of a broad paramagnetic component superimposed by an $[Fe_4S_4]^{2+}$ doublet (we comment in Supporting Information on some aspects of these spectra). The paramagnetic component originates from $[Fe_4S_4]^{1+}$ clusters and is similar to that described by Xia et al. for dithionite-reduced α (*21*). For comparison, we have plotted spectrum 4B from Ni-activated *S10* as a solid line over the dashed-line spectrum 4A from unactivated *S08*. The same spectrum (4B) is plotted as a solid line over the dashed line spectrum 4C from the activated Ti^{3+} citrate-reduced sample *S12*. The spectra are essentially the same except for minor differences in the proportions of the $[Fe_4S_4]^{1+}$ and $[Fe_4S_4]^{2+}$ clusters. This indicates that the cubanes of the A-cluster are insensitive to the presence or absence of Ni_p and Ni_d and to the specific low-potential reductant used (dithionite vs Ti^{3+}citrate). Given that unactivated samples typically contain only ∼0.1 Ni/α, this suggests that occupation of the Ni sites has no discernible influence on the $[Fe_4S_4]^{1+}$ spectral components.

Analysis of the spectra revealed that 65 ± 5% of the $[Fe_4S_4]^{2+}$ clusters in *S08* (spectrum 4A) and *S10* (spectrum 4B) are in the 1+ state, while ca. 35% remained in the 2+ state. One might argue that the dithionite solution potential ($E_0' \sim -540$ mV vs NHE at pH 8) was not low enough to reduce all the clusters. However, a very similar spectral pattern was observed when the more powerful Ti^{3+} citrate (<−800 mV (*47*)) was used (Figure 4C). This suggests that ∼35% of A-clusters reside in an environment that imposes

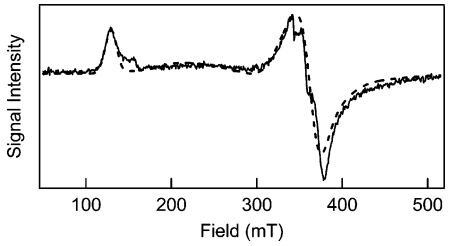

FIGURE 5: EPR Spectrum of Dithionite-Reduced α Subunit. Mössbauer sample *S10* was thawed, transferred to an EPR tube, and refrozen immediately. The spectrum shown (solid line) was obtained at 13 K, using 200 μW microwave power. Other conditions include: microwave frequency, 9.63967 GHz; modulation amplitude, 10.0 G at 100 kHz; average of three scans with conversion time 400 ms and time constant, 100 ms. The dashed line is a composite of $S = 3/2$ and $S = 1/2$ simulations. The $S = 3/2$ simulation assumed 150 μM spin concentration; $E/D = 0.27$ ($\sigma_{E/D} = 0.07$); $D = 2$ cm^{-1}; $g = 2.0, 2.0, 2.0$; and a line width of 30 G. The $S = 1/2$ simulation assumed 60 μM spin concentration; $g = 2.07, 1.89, 1.76$ ($\sigma_g = 0.07, 0, 0.1$); and 100 G line width.

an extremely low $[Fe_4S_4]^{2+/1+}$ cluster potential such that these clusters are not reduced at potentials as low as −800 mV.

The $[Fe_4S_4]^{1+}$ cluster spectra of Ni-activated *S10* exhibit paramagnetic hyperfine structure in zero-applied magnetic field. If the proximal sites of those clusters contained Ni^{1+}, we would expect that exchange interactions between the Fe site to which the bridging Cys is attached (Fe_D in Figure 8 of ref *21*) and the Ni_p^{1+} would yield a system with integer (or zero) electronic spin, in contrast to what is observed. For the A_{red}-CO state which exhibits the NiFeC EPR signal, the exchange coupling was found to be antiferromagnetic, $j \approx 100$ cm^{-1}, in $H = j\mathbf{S}_D \cdot \mathbf{S}_{Ni}$. For the unlikely case that $j = 0$ in the considered $\{[Fe_4S_4]^{1+}, Ni_p^{1+}\}$ distribution, the proximity of the cluster to Ni_p would ensure substantial spin-dipolar interactions which would manifest themselves by the appearance of doublet components characteristic of the 1+ state. These considerations argue against the possibility of an $\{[Fe_4S_4]^{1+}, Ni_p^{1+}\}$ electronic configuration in methylatable samples of α.

We have recorded X-band EPR spectra of an aliquot of the dithionite-reduced sample *S10* of Figure 4B. The spectrum shown in Figure 5 contains two major features. One feature is associated with the $S = 3/2$ form of the $[Fe_4S_4]^{1+}$ cluster. This species is slightly different ($E/D \approx 0.27$ rather than $E/D \approx 0.04$) than that reported (*21*). From spectral simulations and by reference to a Cu^{2+} standard, we obtained an $S = 3/2$ spin concentration of 150 μM spins. The sample contained also an $S = 1/2$ species with rather broad lines (ca. 10 mT) which could be simulated (roughly) with *g*-values 2.06, 1.92, and 1.80, suggesting that the signal results from an $S = 1/2$ $[Fe_4S_4]^{1+}$ cluster rather than from Ni^{1+} (which is expected to have $g_{av} > 2$). This $S = 1/2$ signal has a spin concentration of approximately 60 μM (in 340 μM α). Taking the Mössbauer and EPR information together, this suggests that the sample of Figure 4A contains ∼35% of α subunits with $[Fe_4S_4]^{2+}$, ∼46% with $S = 3/2$ $[Fe_4S_4]^{1+}$, and ∼19% with $S = 1/2$ $[Fe_4S_4]^{1+}$ clusters.

We have also prepared a sample, *S14*, of Ni-activated α in the A_{red}-CO state. A matched sample was prepared for EPR, and as expected, it exhibited the NiFeC signal, with a spin concentration of ≈ 0.15 spins/α. The Mössbauer spectrum of *S14* exhibited at 4.2 K a paramagnetic component representing ∼25% of spectral intensity and a $[Fe_4S_4]^{2+}$ doublet accounting for ∼75% of spectral intensity (Figure 4D). The spectrum of Figure 4D is essentially the same as that presented in Figure 5A of ref *21*). As discussed by Xia et al. (*21*), the paramagnetic component, outlined by the theoretical curve, belongs to $[Fe_4S_4]^{2+}$ clusters exchange-coupled to the Ni_p^{1+} in A_{red}-CO. It is noteworthy that, although the sample contains a large excess of dithionite, all Fe_4S_4 clusters are in the oxidized 2+ state. Thus, the presence of CO changes the potential of $[Fe_4S_4]^{2+/1+}$ clusters such that they become oxidized upon addition of CO (recall that ca. 65% of all clusters are in the 1+ state prior to the addition of CO).

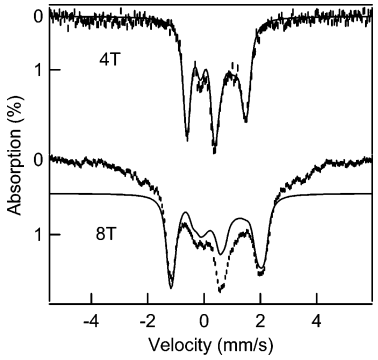

FIGURE 6: The 4.2 K Mössbauer Spectra Recorded in Applied Magnetic Fields. (Top panel) *S04* (activated, no redox agent, methylated). The solid line is a simulation of a single diamagnetic site for an $[Fe_4S_4]^{2+}$ cube with $\Delta E_Q = 1.08$ mm/s, $\eta = 0.5$, and $\delta = 0.45$ mm/s. (Botton panel) *S10* (activated, dithionite-reduced, no substrates). Solid line is a spectral simulation, assuming that 35% of the sample's $[Fe_4S_4]^{2+}$ clusters are diamagnetic. Baseline of the simulation has been shifted vertically to match it with the corresponding feature in the data.

Spectra Recorded in Applied Magnetic Fields. Isolated $[Fe_4S_4]^{2+}$ clusters have a diamagnetic ground state, and thus, spectra taken in applied fields can be fitted by assuming that only the applied field acts at the nucleus. Figure 6 (top spectrum) shows the 4.2 K spectrum of methylated α *S04* recorded in a field of 4.0 T applied parallel to the observed γ radiation. The solid line is a theoretical curve generated by assuming that the cluster ground state is diamagnetic. Within the uncertainties, the assumption of diamagnetism fits the data.

We have shown previously that the $[Fe_4S_4]^{2+}$ cluster in the A_{red}-CO state is exchange-coupled to a Ni^{1+} with CO bound (now designated Ni_p). We have considered whether there is evidence for exchange coupling from an $\{[Fe_4S_4]^{2+} Ni_p^{2+}\}$ assembly in oxidized or methylated samples where Ni_p might be high-spin ($S = 1$), but we find no such evidence. Analyses of spectra of Figure 6 (top spectra) suggest that magnetic hyperfine fields would be at least 14 times smaller than that observed for the A_{red}-CO state, if they existed at all.

Figure 6 (bottom spectrum) shows an 8.0 T spectrum of Ni-activated dithionite-reduced sample *S10* whose low-field spectrum is shown in Figure 4B. The solid line drawn into the spectrum is a theoretical curve for the fraction of α subunits, ca. 35%, that contain an $[Fe_4S_4]^{2+}$ cluster; the simulation assumes strict diamagnetism. From spectral simulations for the $[Fe_4S_4]^{2+}$ cluster component of sample *S10*, we can establish that B_{int} would be less than 0.7 T if

Ni_p^{2+} had $S = 1$. Thus, the data are compatible with either a low-spin Ni_p^{2+} (i.e., no coupling to the $[Fe_4S_4]^{2+}$ cluster) or *very* weak exchange interactions between the $[Fe_4S_4]^{2+}$ cluster and a high-spin Ni^{2+} site.

Acetyl-CoA Synthase Activity in the Absence of a Reductant. We were puzzled by Figure 3 trace C, which seemed to indicate that α has methyl group transfer ability even under conditions of dithionite depletion. This prompted us to conduct an experiment aimed at determining whether an external reductant was actually required for acetyl-CoA synthase activity. The α subunit was methylated with CH_3-Co^{3+}FeSP immediately after addition of dithionite as described in Experimental Procedures. A matched sample but lacking CH_3-Co^{3+}FeSP was prepared concurrently and tested for methyl group transfer activity at different times over a 4 h period. At the end of this period, methyl group transfer activity had ceased, due to the absence of dithionite (equivalent to trace E in Figure 3). Since unmethylated and methylated α consumed dithionite at similar rates, dithionite was most probably consumed in the matched methylated α sample after a 5 h incubation. At that point, CoA and CO were added to the methylated α sample. The resulting solution was incubated for 45 min and then analyzed for acetyl-CoA. In three such experiments, 36, 28, and 31 μM of acetyl-CoA were detected. The NiFeC EPR signal of our α preparations quantifies to 0.1−0.2 spin/α, suggesting that this fraction (or perhaps a slightly higher fraction, e.g., 25% according to the Mössbauer data) of A-cluster in these preparations contain Ni_p. This means that the amount of acetyl-CoA produced in these experiments corresponded to ca. 4 molar equivalents relative to the active A-cluster concentration [(30 μM of acetyl-CoA)/{30 μM α × (0.25Ni_p/α)}]. The specific number of turnovers achieved is less important than the fact that acetyl-CoA was produced in the absence of an external reductant. If an external reductant were required by the enzyme when catalyzing the synthesis of acetyl-CoA, no product would have been produced.

DISCUSSION

A_{ox} and A_{red}-CO. With regard to the oxidized (or A_{ox}) state of the A-cluster, Mössbauer spectra obtained in this study were essentially the same as observed previously (i.e., ∼100% of the Fe_4S_4 clusters were in the 2+ core oxidation state). Given that Ni is predominantly Ni^{2+} under mild redox conditions, and the absence of EPR signals for this state, there is no doubt that A_{ox} contains Ni_p^{2+}. Supporting a Ni^{2+} assignment is a recent XAS and MCD study of the A-cluster in the analogous subunit from *M. thermophila* (see Introduction). That study concluded that Ni_p^{2+} was high-spin $S = 1$ in the A_{ox} state (*22*, *23*). Our results cannot exclude a high-spin assignment, but they suggest that if this were the case, exchange coupling to the $[Fe_4S_4]^{2+}$ cluster would yield internal magnetic fields, B_{int}, that are at least 14 times smaller than those observed for Ni^{1+} contained in the exchange-coupled A_{red}-CO state.

Mössbauer spectra of A_{ox} are essentially insensitive to heterogeneities. Given our other results, it seems likely that heterogeneous populations of A-clusters are present but indistinguishable under nonreducing conditions. Also interesting is that the presence or absence of Ni in these samples (i.e., Ni-activated vs unactivated) had no discernible effect on the Mössbauer spectra; this implies that the heterogeneity is not caused by the occupancy of the proximal site which ought to be devoid of Ni in unactivated samples. Rather, it implies that the redox properties of the cubane are influenced primarily by the protein environment, which itself might be heterogeneous. It is also noteworthy that, in unactivated samples, the cysteinyl sulfur that bridges the Fe_4S_4 cluster with the Ni_p in functional α would probably be coordinated solely to the cluster.

The A_{red}-CO state has been extensively studied (*21*), and our current interest was simply to establish the proportion of functional and nonfunctional A-clusters in the particular batch of α studied here. Similar to the previous study, we observed two components in Mössbauer spectra of samples prepared in this manner, again indicating heterogeneity with ∼25% functional and ∼75% nonfunctional in these batches of α subunit. The 25% spectral component due to the A_{red}-CO state supports our previous assignment of {$[Fe_4S_4]^{2+}$ Ni_p^{1+}-CO}. This assignment is supported by the DFT-computational studies of Brunold (*43*). Thus, in A_{red}-CO, the cubane is in the 2+ state, even though solution potentials are ∼−0.5 V and Ni_p is in the 1+ valence (with CO bound). Assuming that the kinetics of transferring an electron a few angstroms through a cysteinate bridge would be fast, the Ni_p^{1+}-CO unit appears to be thermodynamically incapable of reducing the $[Fe_4S_4]^{2+}$ cubane. This suggests that the $[Fe_4S_4]$ cluster has a very negative thermodynamic reduction potential.

We previously observed that samples of α prepared under a CO atmosphere with a trace of ACS/CODH (added to allow CO to be used as a reductant) contained nonfunctional A-clusters with cubanes in the 2+ core oxidation state, whereas the same cubanes were observed in the 1+ state when samples were prepared in dithionite (*21*). In the present study, a similar phenomenon was observed, using dithionite as the reductant rather than {CO/ACS/CODH}. Since exposure to reductant alone (in the absence of CO) was sufficient to reduce nonfunctional cubanes to the 1+ state, it appears that CO somehow prevents reduction of nonfunctional cubanes to the 1+ state. Possibly the 2+/1+ redox potential of nonfunctional cubanes is shifted from > -0.5 V versus NHE in the absence of CO to < -0.6 V in the presence of CO.

Methylated and Acetylated States CH_3-A_{ox} and $CH_3C(O)$-A_{ox}. Using stopped-flow kinetics, we verified that the methylated sample of α examined had indeed accepted a methyl group from CH_3-Co^{3+}FeSP. Since ca. 100% of $[Fe_4S_4]$ clusters of methylated, Ni-activated A-clusters were found to be in the 2+ core oxidation state, an electronic distribution {$[Fe_4S_4]^{2+}$ Ni_p^{2+}-CH_3} is suggested for the CH_3-A_{ox} state. Similar conclusions were obtained by the EPR study of Barondeau and Lindahl (*36*), as well as by computational studies of Webster et al. (*48*) and Brunold (*43*, *49*). The latter study suggests a highly covalent Ni_p^{2+}-CH_3 moiety contained within an $S = 0$ square-planar configuration (*49*). Assuming this, the electronic ground state of CH_3-A_{ox} would be diamagnetic overall.

Acetylated samples were obtained by thawing the methylated samples and exposing them to CO. We currently cannot verify that the reaction

$$\{[Fe_4S_4]^{2+}\ Ni_p^{2+}\text{-}CH_3\ Ni_d^{2+}\} + CO \rightleftarrows \{[Fe_4S_4]^{2+}\ Ni_p^{2+}\text{-}C(O)CH_3\ Ni_d^{2+}\} \quad (4)$$

occurred. However, unpublished results from our laboratory at Texas A&M University suggest that reaction 4 proceeds to completion under 1 atm CO. Studies from Grahame's and Ragsdale's labs suggest a stable acetyl-intermediate (*35*−*38*). Also, analogous CO insertion reactions of a Ni^{2+}-CH_3 model complex to form an acetyl adduct proceed rapidly (*50*). Assuming that the acetylated state forms, it appears indistinguishable from the methylated form by Mössbauer spectroscopy.

We were surprised that virtually all A-clusters contained $[Fe_4S_4]^{2+}$ cubanes in the solution of α that was incubated with dithionite, then methylated, and frozen quickly; we had expected that the nonfunctional A-clusters, like in dithionite-reduced α, would be in the $[Fe_4S_4]^{1+}$ state. Recall that similar behavior was observed for samples that were reduced with dithionite and exposed to CO; that is, in that case, the $[Fe_4S_4]$ clusters of nonfunctional A-centers became reoxidized upon addition of CO. This suggests that the reduction potential of the cubane ($E^0_{FeS2+/1+}$) for nonfunctional subunits is lowered by the presence of CH_3-Co^{3+}FeSP, to a value below that of dithionite/bisulfite (i.e., ∼−0.5 V vs NHE). This suggests that interactions of α with the corrinoid protein produce a substantial downshift of the $[Fe_4S_4]^{2+/1+}$ cluster potential.

α *Subunits Reduced by Dithionite and by* Ti^{3+} *Citrate.* Ni-activated α subunits develop the capacity to be methylated when they are treated with low-potential reductants such as dithionite or Ti^{3+}citrate. Mössbauer spectra of such samples exhibited two spectral components, namely, a paramagnetic $[Fe_4S_4]^{1+}$ component accounting for ca. 65% of spectral intensity and an $[Fe_4S_4]^{2+}$ component representing 35% of the intensity. These features and proportions were observed regardless of whether α was unactivated (lacking Ni in functional A-centers) or Ni-activated. Thus, this observed heterogeneity in the presence of reductants is not the result of different occupancies of the $\{Ni_p\ Ni_d\}$ binuclear site, but rather is rooted in a heterogeneous distribution of protein conformations. We suspect that A-cluster heterogeneities originate from substantial structural differences on the order of those associated with open and closed α subunit conformations (*15*).

The presence of heterogeneous distributions of A-clusters in overexpressed α subunits, holoenzyme, and the X-ray structure of the holoenzyme impose considerable difficulties on the interpretation of the data (indeed, resolving the heterogeneity problem is one of the major challenges of ACS/CODH research). For the Mössbauer spectra of the A_{red}-CO state, two spectral components with roughly 30/70 population ratio were observed. Extensive previous experiments have demonstrated a heterogeneous A-cluster population, with roughly 30% functional and 70% nonfunctional. On this basis, it seems most reasonable to conclude that *the 30%* $[Fe_4S_4]^{2+}$ *doublet component in dithionite (or* Ti^{3+} *citrate-)-treated* α *subunits arises from functional A-clusters, while the 70%* $[Fe_4S_4]^{1+}$ *paramagnetic component arises from nonfunctional A-clusters.* One might argue that the Fe_4S_4 clusters are only partially reduced by these reductants. However, the reduction potentials of the two reductants used to generate these states differ substantially (ca. −520 mV for dithionite/bisulfite under our experimental conditions and <−800 mV effective reducing ability for Ti^{3+} citrate) such that different proportions of components would be expected if this argument were correct. Similarly, the extent of methylation was independent of reductant used (*46*). The inability of Ti^{3+} citrate to reduce the $[Fe_4S_4]^{2+}$ cluster of functional A-clusters suggests that they have an extremely low $[Fe_4S_4]^{2+/1+}$ reduction potential. Ti^{3+} citrate readily reduces the $[Fe_4S_4]^{1+}$ cluster of the nitrogenase Fe protein to the all-ferrous $[Fe_4S_4]^0$ state, and the 1+/0 potential of the Fe protein has been determined to be <−0.8 V vs NHE (*47*). Our results suggest that the 2+/1+ reduction potential for the $[Fe_4S_4]$ cluster in functional α subunits is more negative than that. Consistent with this is the inability of Ni^{1+} (a known powerful reductant) to reduce the $[Fe_4S_4]^{2+}$ cluster of functional A-clusters in the A_{red}-CO state.

Since CO and methyl groups are thought to bind to Ni_p, we are particularly interested in the electronic properties of the noncubane $\{Ni_p\ Ni_d\}$ portion of functional A-clusters in the reductant-treated state. Given that we can observe with Mössbauer spectroscopy only the $[Fe_4S_4]$ cluster, our ability to draw conclusions in this regard is limited. Most fundamentally, we do not know the oxidation state of Ni_p in reductant-treated functional A-clusters. In the following, we consider three scenarios.

The first scenario has Ni_p of reductant-treated functional A-clusters in the 2+ state; That is, the electronic configuration would be that of A_{ox}. Since the A_{ox} state cannot be methylated, reductant-treated enzyme would not be activated for methylation. The possibility that reductive activation occurs only after CH_3-Co^{3+}FeSP docks to the α subunit is quite appealing as it might prevent loss of reducing equivalents in the absence of CH_3-Co^{3+}FeSP, a strategy reminiscent of that used, for instance, by cytochrome P450 (*53*).

In the second scenario, Ni_p in reductant-treated functional A-clusters would attain the 1+ state; that is, the electronic configuration would be that of A_{red}-CO state but without CO bound. For an $\{[Fe_4S_4]^{2+}\ Ni_p^{1+}\}$ configuration, an EPR signal typical of Ni^{1+} would have been observed for any reasonable exchange coupling between the Ni^{1+} and the $[Fe_4S_4]^{2+}$ cluster. The possibility of an $\{[Fe_4S_4]^{2+}\ Ni_p^{1+}\}$ configuration for the reductively activated state is further discounted by the Mössbauer and EPR spectroscopic properties of the methylated intermediate. The absence of an EPR signal attributable to the A-cluster in methylated samples and the presence of $[Fe_4S_4]^{2+}$ cubanes suggest that Ni_p is in the 2+ oxidation state (and with the methyl group bound).

Prior to the present study, another possibility considered within the context of the second scenario was that catalysis only occurs in the presence of an external redox shuttle (*6*). In this case, electrons from the external reductant would transfer to the A-cluster during one step of catalysis (e.g., to a transiently formed Ni_p^{3+}-$C(O)CH_3$ species) and then return to the external oxidant during a later step (e.g., upon formation of product) to complete the catalytic cycle. Our demonstration that α can turn over in the absence of an external reductant indicates that no such redox shuttle is

required for catalysis. Our observation of multiple turnovers suggests that the reducing equivalents generated at the end of a catalytic cycle are retained by the enzyme. This experiment also shows that α can turn over *without* attaining the A_{red}-CO state. Thus, as the α subunit was methylated in the absence of CO, the A_{red}-CO state could not have formed in that step. CO and CoA were added to the methylated intermediate, but only after dithionite had been exhausted. The A_{red}-CO state has only been observed with the α subunit in solutions containing a low-potential reductant, and so the A_{red}-CO state could not have formed in that last step. Nevertheless, product was detected. Thus, the enzyme appears to have gone through all necessary steps of catalysis without sampling the A_{red}-CO state, leading us to conclude that *the A_{red}-CO state is not a required catalytic intermediate*.

In the third scenario, the reductant-treated functional A-clusters would attain the electronic configuration $\{[Fe_4S_4]^{2+}\ Ni_p^0\}$, either in the presence or absence of CoFeSP. Since Ni^0 is d^{10} and thus diamagnetic, A-clusters in this state would not exhibit an EPR signal and the Mössbauer spectra would exhibit the $[Fe_4S_4]^{2+}$ doublet (as observed). A reasonable objection to this scenario is the existence of an $[Fe_4S_4]^{2+}$ cluster spatially located close to the powerful reductant, Ni_p^0. One would perhaps expect that the $\{[Fe_4S_4]^{2+}\ Ni_p^0\}$ distribution would spontaneously transfer an electron, producing a $\{[Fe_4S_4]^{1+}\ Ni_p^{1+}\}$ distribution. Indeed, the density functional theory studies of Schenker and Brunold (*43*) and Field (*54*) suggest this. However, our Mössbauer results indicate that the $\{[Fe_4S_4]^{1+}\ Ni_p^{1+}\}$ distribution is not present in reductively activated or methylatable forms of the enzyme. Reduction potentials for the $[Fe_4S_4]^{2+/1+}$ and $Ni_p^{1+/0}$ couples (E^0_{FeS} vs $E^0_{Ni1+/0}$) will dictate the relative stability of these two distributions. The relevant potentials are not known, and they are expected to depend strongly on coordination environments and protein environmental effects (e.g., open vs closed conformation of α). Such difficult-to-quantify factors would be equally difficult to assess in computational studies. Consideration of such factors have been shown to be required to approximate experimental reduction potentials of simple isolated $[Fe_4S_4]^{2+/1+}$ couples using DFT calculations (*55*). Given the complexity of the A-cluster and its environment, we suspect that calculating analogous potentials for the subcomponents of the A-cluster will be critical in assessing the feasibility of a $\{[Fe_4S_4]^{2+}\ Ni_p^0\}$ distribution.

Given the general agreement that the electronic distribution of the A_{red}-CO state is $\{[Fe_4S_4]^{2+}\ Ni_p^{1+}$-CO$\}$, it would appear that $E^0_{FeS} < E^0_{Ni2+/1}$ in that state (including the effect of CO binding, which may be substantial in stabilizing the 1+ state). Given our inability to reduce the Fe_4S_4 clusters with Ti^{3+} citrate, it is not implausible that $E^0_{FeS} < E^0_{Ni1+/0}$ for the reductively activated state, as would be required for a stable $\{[Fe_4S_4]^{2+}\ Ni_p^0\}$ distribution. Moreover, we have presented evidence here that E^0_{FeS} of *nonfunctional* A-clusters *declines* upon exposure to either CO or CH_3-Co^{3+}FeSP, such that the cubane remains in the 2+ state in the presence of strong reductants such as dithionite and Ti^{3+} citrate. E^0_{FeS} for *functional* A-clusters may be permanently at this lower value. Redox potentials of $[Fe_4S_4]^{2+/1+}$ clusters can be so negative that the clusters are essentially irreducible, as shown for the cluster in endonuclease III from *E. coli* (*56*) and mutants of *Azotobacter vinelandii* Ferredoxin I (*57*). The other metal ion bridged to Ni_p, namely, Ni_d^{2+}, appears similarly resistant

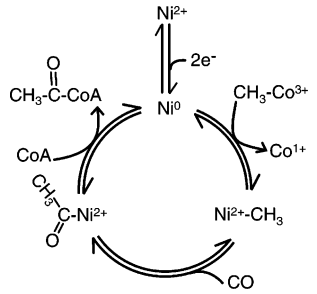

FIGURE 7: Proposed Mechanism of ACS Catalysis. The Ni in the figure reflects proximal Ni_p. Both the distal Ni_d and Fe_4S_4 cubane are presumed to remain in the 2+ oxidation states during each step of catalysis.

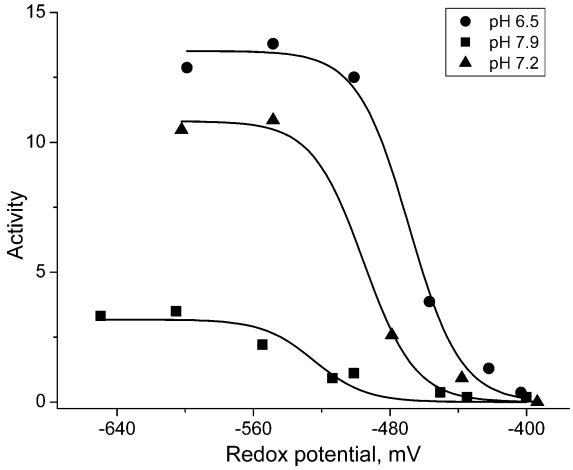

FIGURE 8: Global Best-Fit of Nernst Equation to Data of Bhaskar et al. (*38*). The fitting is described in Experimental Procedures. One data point each at ~−650 mV vs NHE was excluded from the pH 6.5 and 7.2 datasets, as these points reflect a separate inactivation process.

to reduction to the 1+ state (*2*, *15*). This raises the possibility that the inability to reduce the metal ions bridging Ni_p somehow contributes to stabilizing the biologically unprecedented Ni_p^0 state. Protonation of cysteinyl residues (and perhaps the binding of CoFeSP) may also contribute to stabilizing this state.

Implications for the ACS Catalytic Mechanism. Our results favor the mechanism shown in Figure 7. The activation step could occur either independently of the CoFeSP or perhaps only when this protein has docked to the α subunit (*4*). In either case, the mechanism involves a two-electron activation of A_{ox} without reduction of the $[Fe_4S_4]^{2+}$ cluster. The reductively activated state accepts a methyl group from CH_3-Co^{3+}FeSP followed by CO insertion, forming the acetyl intermediate. Finally, CoA attacks, forming product and regenerating the reductively activated state.

Bhaskar et al. (*38*) measured the activity of a homologue A-cluster-containing enzyme from *Methanosarcina barkeri* as a function of solution electrochemical potential and reported that a one-electron reductive activation ($n = 1$) fitted their data best. However, we fitted globally the Nernst equation to all three data sets of Bhaskar et al. and obtained $n = 1.7 \pm 0.2$, with $E_0' = -469$, -495, and -524 mV, for data sets collected at pH 6.5, 7.2, and 7.9, respectively (Figure 8). Thus, the data of Bhaskar actually *support* a two-electron reductive activation process rather than an $n = 1$ process as reported. Also interesting is the pH dependence

of the apparent midpoint potentials (~40 mV/pH), as this implies that reductive activation involves protonation. Protonating a cysteinate ligand of Ni_p would neutralize it and lessen the thermodynamic difficulty of reducing Ni^{2+} ions (*58*). A similar situation may exist for the Ni ion in NiFe hydrogenases (*59*, *60*).

In a separate study of ACS/CODH from *M. thermoacetica*, Lu and Ragsdale (*41*) concluded that the reductively activated state is 1 electron more reduced than A_{ox} based as well on a plot of activity as a function of solution electrochemical potential. The model that assumed a one-electron reductive activation ($n = 1$) fitted the data best. We have re-fitted the Nernst equation to these data similar to our treatment of the Bhaskar et al. data and verified that an $n = 1$ model (with $E_0' = -486$ mV vs NHE, pH 7.0) fits the data best. Thus, the $n = 1$ value obtained in that study stands in conflict with the mechanism presented above and the results of Bhaskar et al. (*38*).

We realize that additional evidence for the Ni_p^0 species suggested in our mechanism is required. Nevertheless, A-cluster model compounds containing Ni_p-like Ni^0 species have been reported (*61*, *62*), and other Ni^0-based complexes are known to exhibit similar reaction chemistry to that carried out by this enzyme (*50*). When the results presented here are included, the possibility that such an unprecedented redox state of Ni might be attained in an enzyme deserves further serious consideration.

SUPPORTING INFORMATION AVAILABLE

Further comments regarding the analysis of the spectra of Figure 4. This material is available free of charge via the Internet at http://pubs.acs.org.

REFERENCES

1. Drennan, C. L., Doukov, T. I., and Ragsdale, S. W. (2004) The metalloclusters of carbon monoxide dehydrogenase/acetyl-CoA synthase: a story in pictures, *J. Biol. Inorg. Chem. 9*, 511−515.
2. Lindahl, P. A. (2004) Acetyl-coenzyme A synthase: the case for a $Ni_p(0)$-based mechanism of catalysis, *J. Biol. Inorg. Chem. 9*, 516−524.
3. Volbeda, A., and Fontecilla-Camps, J. C. (2004) Crystallographic evidence for a CO/CO_2 tunnel gating mechanism in the bifunctional carbon monoxide dehydrogenase/acetyl coenzyme A synthase from *Moorella thermoacetica*, *J. Biol. Inorg. Chem. 9*, 525−532.
4. Brunold, T. C. (2004) Spectroscopic and computational insights into the geometric and electronic properties of the A-cluster of acetyl-coenzyme A synthase, *J. Biol. Inorg. Chem. 9*, 533−541.
5. Riordan, C. G. (2004) Synthetic chemistry and chemical precedents for understanding the structure and function of acetyl coenzyme A synthase, *J. Biol. Inorg. Chem. 9*, 542−549.
6. Ragsdale, S. W. (2004) Life with carbon monoxide, *Crit. Rev. Biochem. Mol. 39*, 165−195.
7. Hegg, E. L. (2004) Unraveling the structure and mechanism of acetyl-coenzyme A synthase, *Acc. Chem. Res. 37*, 775−783.
8. Lindahl, P. A., and Chang, B. (2001) The evolution of acetyl-CoA synthase, *Origins Life Evol. Biosphere 31*, 403−434.
9. Lindahl, P. A. (2002) The Ni-containing carbon monoxide dehydrogenase family: light at the end of the tunnel? *Biochemistry 41*, 2097−2105.
10. Lebertz, H., Simon, H., Courtney, L. F., Benkovic, S. J., Zydowsky, L. D., Lee, K., and Floss, H. G. (1987) Stereochemistry of acetic acid formation from 5-methyltetrahydrofolate by *Clostridium thermoaceticum*, *J. Am. Chem. Soc*, *109*, 3173−3174.
11. Kumar, M., Qiu, D., Spiro, T., and Ragsdale, S. W. (1995) A methylnickel intermediate in a bimetallic mechanism of acetyl-Coenzyme A synthesis by anaerobic bacteria, *Science 270*, 628−630.
12. Loke, H. K., Tan, X., and Lindahl, P. A. (2002) Genetic construction of truncated and chimeric metalloproteins derived from the alpha subunit of acetyl-CoA synthase from *Clostridium thermoaceticum*, *J. Am. Chem. Soc. 124*, 8667−8672.
13. Tan, X., Sewell, C., Yang, Q., and Lindahl, P. A. (2003) Reduction and methyl transfer kinetics of the alpha subunit from acetyl coenzyme A synthase, *J. Am. Chem. Soc. 125*, 318−319.
14. Doukov, T. I., Iverson, T. M., Seravalli, J., Ragsdale, S. W., and Drennan, C. L. (2002) A Ni−Fe−Cu center in a bifunctional carbon monoxide dehydrogenase/acetyl-CoA synthase, *Science 298*, 567−572.
15. Darnault, C., Volbeda, A., Kim, E. J., Legrand, P., Vernède, X., Lindahl, P. A., and Fontecilla-Camps, J. C. (2003) Ni-Zn-[Fe-4-S-4] and Ni-Ni-[Fe-4-S-4] clusters in closed and open subunits of acetyl-CoA synthase/carbon monoxide dehydrogenase, *Nat. Struct. Biol. 10*, 271−279.
16. Svetlitchnyi, V., Dobbek, H., Meyer-Klaucke, W., Meins, T., Thiele, B., Romer, P., Huber, R., and Meyer, O. (2004) A functional Ni-Ni-[4Fe-4S] cluster in the monomeric acetyl-CoA synthase from *Carboxydothermus hydrogenoformans*, *Proc. Natl. Acad. Sci. U.S.A. 101*, 446−451.
17. Krüger, H. J., Peng, G., and Holm, R. H. (1991) Low-potential Nickel(III,II) complexes−new systems based on tetradentate amidate thiolate ligands and the influence of ligand structure on potentials in relation to the nickel site in [NiFe] hydrogenases, *Inorg. Chem. 30*, 734−742.
18. Hanss, J., and Kruger, H. J. (1998) First isolation and structural characterization of a nickel(III) complex containing aliphatic thiolate donors, *Angew. Chem., Int. Ed. 37*, 360−363.
19. Marlin, D. S., and Mascharak, P. K. (2000) Coordination of carboxamido nitrogen to tervalent iron: insight into a new chapter of iron chemistry, *Chem. Soc. Rev. 29*, 69−74.
20. Harrop, T. C., Olmstead, M. M., and Mascharak, P. K. (2002) Novel folding of *N,N′*-naphthalenebis(o-mercaptobenzamide) in nickel(II) complexes: monomeric and trimeric species with unexpected 'butterfly' and 'slant chair' structure, *Inorg. Chim. Acta 338*, 189−195.
21. Xia, J. Q., Hu, Z. G., Popescu, C. V., Lindahl, P. A., and Münck, E. (1997) Mössbauer and EPR study of the Ni-activated alpha-subunit of carbon monoxide dehydrogenase from *Clostridium thermoaceticum*, *J. Am. Chem. Soc. 119*, 8301−8312.
22. Gu, W. W., Gencic, S., Cramer, S. P., and Grahame, D. A. (2003) The A-cluster in subunit β of the acetyl-CoA decarbonylase/synthase complex from *Methanosarcina thermophila*: Ni and FeK-Edge XANES and EXAFS analyses, *J. Am. Chem. Soc. 125*, 15343−15351.
23. Funk, T., Gu, W. W., Friedrich, S., Wang, H. X., Gencic, S., Grahame, D. A., and Cramer, S. P. (2004) Chemically distinct Ni sites in the A-cluster in subunit β of the Acetyl-CoA decarbonylase/synthase complex from *Methanosarcina thermophila*: Ni L-edge absorption and X-ray magnetic circular dichroism analyses, *J. Am. Chem. Soc. 126*, 88−95.
24. Xia, J. Q., and Lindahl, P. A. (1996) Assembly of an exchange-coupled $[Ni:Fe_4S_4]$ cluster in the α metallosubunit of carbon monoxide dehydrogenase from *Clostridium thermoaceticum* with spectroscopic properties and CO-binding ability mimicking those of the acetyl-CoA synthase active site, *J. Am. Chem. Soc. 118*, 483−484.
25. Russell, W. K., Stålhandske, C. M. V., Xia, J. Q., Scott, R. A., and Lindahl, P. A. (1998) Spectroscopic, redox, and structural characterization of the Ni-labile and nonlabile forms of the acetyl-CoA synthase active site of carbon monoxide dehydrogenase, *J. Am. Chem. Soc. 120*, 7502−7510.
26. Ragsdale, S. W., Ljungdahl, L. G., and Dervartanian, D. V. (1982) Electron paramagnetic resonance evidence for nickel-substrate interaction in carbon monoxide dehydrogenase from *Clostridium thermoaceticum*, *Biochem. Biophys. Res. Commun. 108*, 658−663.
27. Ragsdale, S. W., Ljungdahl, L. G., and Dervartanian, D. V. (1983) C-13 and Ni-61 Isotope substitutions confirm the presence of a Nickel(III)-carbon species in acetogeneic CO dehydrogenases, *Biochem. Biophys. Res. Commun. 115*, 658−665.
28. Ragsdale, S. W., Wood, H. G., and Antholine, W. E. (1985) Evidence that an iron−nickel carbon complex is formed by reaction of CO with the CO dehydrogenase from *Clostridium thermoaceticum*, *Proc. Natl. Acad. Sci. U.S.A.* 82, 6811−6814.
29. Lindahl, P. A., Münck, E., and Ragsdale, S. W. (1990) CO dehydrogenase from *Clostridium thermoaceticum*−EPR and elec-

trochemistry studies in CO_2 and argon atmospheres, *J. Biol. Chem. 265*, 3873−3879.
30. Lindahl, P. A., Ragsdale, S. W., and Münck, E. (1990) Mössbauer study of CO dehydrogenase from *Clostridium thermoaceticum*, *J. Biol. Chem. 265*, 3880−3888.
31. Shin, W., and Lindahl, P. A. (1992) Discovery of a labile nickel ion required for CO acetyl-CoA exchange activity in the NiFe complex of carbon monoxide dehydrogenase from *Clostridium thermoaceticum*, *J. Am. Chem. Soc. 114*, 9718−9719.
32. Shin, W. S., Anderson, M. E., and Lindahl, P. A. (1993) Heterogeneous nickel environments in carbon monoxide dehydrogenase from *Clostridium thermoaceticum*, *J. Am. Chem. Soc. 115*, 5522−5526.
33. Shin, W., and Lindahl, P. A. (1993) Low spin quantitation of NiFeC EPR signal intensity from carbon monoxide dehydrogenase is not due to damage incurred during protein purification, *Biochem. Biophys. 1161*, 317−322.
34. Fraser, D. M., and Lindahl, P. A. (1999) Stoichiometric CO reductive titrations of acetyl-CoA synthase (carbon monoxide dehydrogenase) from *Clostridium thermoaceticum*, *Biochemistry 38*, 15697−15705.
35. Grahame, D. A., Khangulov, S., and DeMoll, E. (1996) Reactivity of a paramagnetic enzyme-CO adduct in acetyl-CoA synthesis and cleavage, *Biochemistry 35*, 593−600.
36. Barondeau, D. P., and Lindahl, P. A. (1997) Methylation of carbon monoxide dehydrogenase from *Clostridium thermoaceticum* and mechanism of acetyl coenzyme A synthesis, *J. Am. Chem. Soc. 119*, 3959−3970.
37. Seravalli, J., Kumar, M., and Ragsdale, S. W. (2002) Rapid kinetic studies of acetyl-CoA synthesis: Evidence supporting the catalytic intermediacy of a paramagnetic NiFeC species in the autotrophic Wood-Ljungdahl pathway, *Biochemistry 41*, 1807−1819.
38. Bhaskar B., DeMoll, E., and Grahame, D. A. (1998) Redox-dependent acetyl transfer partial reaction of the acetyl-CoA decarbonylase/synthase complex: kinetics and mechanism, *Biochemistry 37*, 14491−14499.
39. Pezacka, E., and Wood, H. G. (1988) Acetyl-CoA pathway of autotrophic growth—identification of the methyl binding site of the CO dehydrogenase, *J. Biol. Chem. 263*, 16000−16003.
40. Lu, W.-P., Harder, S. R., and Ragsdale, S. W. (1990) Controlled potential enzymology of methyl transfer reactions involved in acetyl-CoA synthesis by CO dehydrogenase and the corrinoid iron sulfur protein from *Clostridium thermoaceticum*, *J. Biol. Chem. 265*, 3124−3133.
41. Lu, W. P., and Ragsdale, S. W. (1991) Reductive activation of the coenzyme A acetyl-CoA isotopic exchange reaction catalyzed by carbon monoxide dehydrogenase from *Clostridium thermoaceticum* and its inhibition by nitrous oxide and carbon monoxide, *J. Biol. Chem. 266*, 3554−3564.
42. Ragsdale, S. W., and Kumar, M. (1996) Nickel-containing carbon monoxide dehydrogenase/acetyl-CoA synthase, *Chem. Rev. 96*, 2515−2539.
43. Schenker, R. P., and Brunold, T. C. (2003) Computational studies on the A cluster of acetyl-coenzyme A synthase: geometric and electronic properties of the NiFeC species and mechanistic implications, *J. Am. Chem. Soc. 125*, 13962−13963.
44. Seefeldt, L. C., and Ensign, S. A. (1994) A continuous, spectrophotometric activity assay for nitrogenase using the reductant Titanium(III) citrate, *Anal. Biochem. 221*, 379−386.
45. Pelley, J. W., Garner, C. W., and Little, G. H. (1978) Simple rapid Biuret method for estimation of protein in samples containing thiols, *Anal. Biochem. 86*, 341−343.
46. Tan, X., Sewell, C., and Lindahl, P. A. (2002) Stopped-flow kinetics of methyl group transfer between the corrinoid-iron-sulfur protein and acetyl-coenzyme A synthase form *Clostridium thermoaceticum*, *J. Am. Chem. Soc. 124*, 6277−6284.
47. Guo, M. L., Sulc, F., Ribbe, M. W., Farmer, P. J., and Burgess, B. K. (2002) Direct assessment of the reduction potential of the $[4Fe-4S]^{1+/0}$ couple of the Fe protein from *Azotobacter vinelandii*, *J. Am. Chem. Soc. 124*, 12100−12101.
48. Webster, C. E., Darensbourg, M. Y., Lindahl, P. A., and Hall, M. B. (2004) Structures and energetics of models for the active site of acetyl-coenzyme a synthase: role of distal and proximal metals in catalysis, *J. Am. Chem. Soc. 126*, 3410−3411.
49. Schenker, R., Mock, M. T., Kleber-Emmons, M. T., Riordan, C. G., and Brunold, T. C. (2005) Spectroscopic and computational studies on $[Ni(tmc)CH_3]OTf$: implications for Ni-methyl bonding in the A cluster of acetyl-CoA synthase, *Inorg. Chem. 44*, 3605−3517.
50. Hsiao, Y.-M., Chojnacki, S. S., Hinton, P., Reibenspies, J. H., and Darensbourg, M. Y. (1993) Organometallic chemistry of sulfur phosphorus donor ligand complexes of Nickel(II) and Nickel(0). *Organometallics 12*, 870−875.
51. Lindahl, P. A., Day, E. P., Kent, T. A., Orme-Johnson, W. H., and Münck, E. (1985) Mössbauer, electron paramagnetic resonance, and magnetization studies of the *Azotobacter vinelandii* Fe protein—evidence for a $[Fe_4S_4]^{1+}$ cluster with spin $S = 3/2$, *J. Biol. Chem. 260*, 1160−1173.
52. Hagen, W. R., van den Berg, W. A. M., van Dongen, W. M. A. M., Reijerse, E. J., and van Kan, P. J. M. (1998) EPR spectroscopy of biological iron−sulfur clusters with spin-admixed $S = 3/2$ ground states, *J. Chem. Soc. Faraday Trans. 94*, 2969−2973.
53. Sligar, S. G. (1976) Coupling of spin, substrate, and redox equilibria in cytochrome P450, *Biochemistry* 15, 5399−5406.
54. Amara, P., Volbeda, A., Fontecilla-Camps, J. C., and Field, M. J. (2005) A quantum chemical study of the reaction mechanism of acetyl-coenzyme A synthase, *J. Am. Chem. Soc. 127*, 2776−2784.
55. Torres, R. A., Lovell, T., Noodleman, L., and Case, D. A. (2003) Density functional-and reduction potential calculations of Fe_4S_4 clusters, *J. Am. Chem. Soc. 125*, 1923−1936.
56. Cunningham, R. P., Asahara, H., Bank, J. F., Scholes, C. P., Salerno, J. C., Surerus, K., and Münck, E. (1989) Endonuclease-III is an iron sulfur protein, *Biochemistry 28*, 4450−4455.
57. Iismaa, S. E., Vazquez, A. E., Jensen, G. M., Stephens, P. J., Butt, J. N., Armstrong, F. A., and Burgess, B. K. (1991) Site-directed mutagenesis of *Azotobacter vinelandii* Ferredoxin I: changes in [4Fe-4S] cluster reduction potential and reactivity, *J. Biol. Chem. 266*, 21563−21571.
58. Farmer, P. J., Reibenspies, J. H., Lindahl, P. A., and Darensbourg, M. Y. (1993) Effects of sulfur site modification on the redox potentials of derivatives of [*N*,*N*′-bis(2-mercaptoethyl)-1,5-diazacyclooctanoto]Nickel(II), *J. Am. Chem. Soc. 115*, 4665−4674.
59. Jones, A. K., Lamle, S. E., Pershad, H. R., Vincent, K. A., Albracht, S. P. J., and Armstrong, F. A. (2003) Enzyme electrokinetics: electrochemical studies of the anaerobic interconversions between active and inactive states of *Allochromatium vinosum* [NiFe]-hydrogenase, *J. Am. Chem. Soc. 125*, 8505−8514.
60. Amara, P., Volbeda, A., Fontecilla-Camps, J. C., and Field, M. J. (1999) A hybrid density functional theory molecular mechanics study of nickel−iron hydrogenase: Investigation of the active site redox states, *J. Am. Chem. Soc. 121*, 4468−4477.
61. Linck, R. C., Spahn, C. W., Rauchfuss, T. B., and Wilson, S. R. (2003) Structural analogues of the bimetallic reaction center in acetyl CoA synthase: A Ni−Ni model with bound CO, *J. Am. Chem. Soc. 125*, 8700−8701.
62. Krishnan, R., and Riordan, C. G. (2004) Cys-Gly-Cys tripeptide complexes of nickel: binuclear analogues for the catalytic site in acetyl coenzyme A synthase, *J. Am. Chem. Soc. 126*, 4484−4485.
63. Watt, G. D., and Reddy, K. R. N. (1994) Formation of an all ferrous Fe_4S_4 cluster in the iron protein component of *Azotobacter vinelandii* nitrogenase, *J. Inorg. Biochem. 53*, 281−294.
64. McKenna, C. E., Menard, D., Dao, C. J., Stephens, P. J., and McKenna, M. C. (1988) In *Nitrogen Fixation: Hundred Years After* (Bothe, H., de Bruijn, F. J., and Newton, W. E., Eds.) pp 131, Gustav Fischer, New York.

BI060003+